Amino Acids (2015) 47:987–995
DOI 10.1007/s00726-015-1927-z

ORIGINAL ARTICLE

Manganese superoxide dismutase from human pathogen *Clostridium difficile*

Wei Li · Hongfei Wang · Cheng Lei · Tianlei Ying · Xiangshi Tan

Received: 18 December 2013 / Accepted: 21 January 2015 / Published online: 6 February 2015

Abstract *Clostridium difficile* is a human pathogen that causes severe antibiotic-associated *Clostridium difficile* infection (CDI). Herein the $MnSOD_{cd}$ from *C. difficile* was cloned, expressed in *Escherichia Coli*,and characterized by X-ray crystallography, UV/Vis and EPR spectroscopy, and activity assay, et al. The crystal structure of $MnSOD_{cd}$ (2.32 Å) reveals a manganese coordination geometry of distorted trigonal bipyramidal, with His111, His197 and Asp193 providing the equatorial ligands and with His56 and a hydroxide or water forming the axial ligands. The catalytic activity of $MnSOD_{cd}$ (8,600 U/mg) can be effectively inhibited by 2-methoxyestradiol with an IC_{50} of 75 μM. The affinity investigation between 2-methoxyestradiol and $MnSOD_{cd}$ by ITC indicated a binding constant of 8.6 μM with enthalpy changes ($\Delta H = -4.08 \pm 0.03$ kcal/mol, $\Delta S = 9.53 \pm 0.02$ cal/mol/deg). An inhibitory mechanism of $MnSOD_{cd}$ by 2-methoxyestradiol was probed and proposed based on molecular docking models and gel filtration analysis. The 2-methoxyestradiol may bind $MnSOD_{cd}$ to interfere with the cross-linking between the two active sites of the dimer enzyme, compromising the SOD activity. These results provide valuable insight into the rational design of $MnSOD_{cd}$ inhibitors for potential therapeutics for CDI.

Keywords MnSOD · Crystal structure · Superoxide dismutase · *Clostridium difficile* · 2-Methoxyestradiol

Introduction

Clostridium difficile, which inhabits human digestive tract, is an anerobic gram-positive spore-forming human pathogen (Kuehne et al. 2010). It can produce toxins A and B, and causes an acute illness called *Clostridium difficile* infection (CDI) in humans, with symptoms ranging from severe diarrhea, antibiotic-associated colitis, pseudomembranous colitis, toxic megacolon, intestinal perforations, and ultimately to death (Rupnik et al. 2009). The incidence and severity of CDI have been increasing since 2002, which caused hospital outbreaks with high morbidity and mortality in North America and Europe (Williams and Spencer 2009). The current main treatments for CDI are oral antibiotics vancomycin and metronidazole (Scheinfeld and Biggers 2008). However, those antibiotics have been implicated as actual risk factors for CDI and have a considerable CDI recurrence rate up to 35 % (Koo et al. 2010). The management of these multiple recurrences has become one of the toughest challenges for CDI treatments. Therefore, new therapies of CDI, with new drug-target enzymes and antibiotics are desperately needed (Sebaihia et al. 2006).

Handling Editor: F. Hollfelder.

Electronic supplementary material The online version of this article (doi:10.1007/s00726-015-1927-z) contains supplementary material, which is available to authorized users.

W. Li
Institutes of Biomedical Sciences, Fudan University, Shanghai 200433, China

H. Wang
State Key Laboratory of Quantum Optics and Quantum Optics Devices, Shanxi University, Taiyuan 030006, China

C. Lei · T. Ying
Department of Chemistry, Fudan University, Shanghai 200433, China

X. Tan (✉)
Department of Chemistry and Institutes of Biomedical Sciences, Fudan University, Shanghai 200433, China
e-mail: xstan@fudan.edu.cn

The virulent surface proteins, toxin A and toxin B, produced by *C. difficile* are demonstrated to induce mitochondrial swelling and release of reactive oxygen species (ROS) in cells (He et al. 2000). ROS are also produced from the severe inflammatory cascade elicited by the internalization of toxin A into infected cells (He et al. 2002). The substantial amounts of ROS would deeply attack the host cells and facilitate the infection of *C. difficile* (Fisher and Naughton 2005). However, ROS, as a double-edged sword, can also place *C. difficile* itself at the oxidative stress state. The microbial superoxide dismutase (SOD), which catalyzes the dismutation of $O_2^{\bullet -}$ to generate H_2O_2 and O_2, is an important member in the first line of defensive protection microbe from oxidative damage (Fridovich 2011). Lots of examples demonstrated that activity of SODs for pathogenic bacteria may relate to their virulence (Mallery et al. 2004; Ambrose and Gatti 2013). Based on the metal cofactors, SODs were classed into three groups, which include Cu/Zn-SOD (Zhang and Zhu 2006); MnSOD and the high homologous FeSOD (Chambergo et al. 2012) and NiSOD (Herbst et al. 2009). *Clostridium difficile* genome contains sodA, which is a putative MnSOD.

Herein, for the first time, the $MnSOD_{cd}$ from *C. difficile* was cloned, expressed in *Escherichia coli*,and characterized by X-ray crystallography, UV/Vis and EPR spectroscopy, and SOD activity assay, et al. 2-methoxyestradiol, a physiologic metabolite of the endogenous estrogen 17 β-estradiol, has been identified to possess SOD activity inhibitory ability (Huang et al. 2000). Moreover, 2-methoxyestradiol has been recently approved in clinical phase two by FDA, allowing its use for the treatment of ovarian cancer (Florczak et al. 2009). In this study, the inhibition of $MnSOD_{cd}$ by 2-methoxyestradiol was investigated, and the binding affinity of 2-methoxyestradiol with $MnSOD_{cd}$ was measured by isothermal titration calorimetry (ITC). The inhibitory model of $MnSOD_{cd}$ by 2-methoxyestradiol based on molecular docking simulation and gel fitration analysis was proposed and discussed.

Materials and methods

Cloning, expression and purification of $MnSOD_{cd}$

The $MnSOD_{cd}$ gene was amplified from *C. difficile* genomic DNA using a pair of primers:5′-TA**GGATCC**CCTGAAAA TAACAAATTTAAGG-3′(F); 5′-CC**CTCGAG**TTAATCTT GAGATTTTAAATTTTTG-3′(R). The PCR products digested *by BamH* I and *Xho* I (New England Biolabs) were ligated into the linearized MBPHT-mCherry2 vector with an N-terminal maltose-binding protein followed by an 8 × histidine tag and TEV protease cleavage site. The resulting ligation mixture was transformed into XL10-Gold competent cells (Novagen) by heat shock. The recombination plasmid was verified by DNA sequencing (Invitrogen) and transformed into Rosseta (DE3) pLysS competent cells (Novagen), which grew in modified LB media containing 50 μg/mL ampicillin and 34 μg/mL chloramphenicol with vigorous shaking at 37 °C until an OD_{600} of 0.6 was attained. The expression was induced with the addition of 0.3 mM isopropyl-1-thio-D-galactopyranoside (IPTG) and further incubated at 37 °C for 8 h. Cells were collected by centrifugation at 4,500×*g* for 10 min at 4 °C in a Sorvall (model RC-6C Plus) swinging bucket centrifuge. Cell pellets were resuspended in 20 mM potassium phosphate, pH 7.4, 25 mM imidazole, 500 mM NaCl, 1 mM PMSF. Then the cells were sonicated and centrifuged at 12,000×*g* for 30 min to clarify the lysate. The lysate was purified by a preformed Ni–NTA His-Trap gravity column (Qiagen, Chatsworth, CA). SOD_{cd} fractions were then tested for initial purity by SDS-PAGE and subjected to TEV protease for incision. After cleavage of the N-terminal maltose-binding protein (MBP) tag, the protein solution was subjected to Ni–NTA column again to remove the MBP tag. Pure (>85 %) fractions were combined, and subjected to the ÄKTA *purifier* FPLC system (Amersham Biosciences) and passed over a HiLoad™ 16/60 Superdex™ 200 gel filtration column (GE health). Fractions were analyzed by SDS-PAGE (which indicated >95 % purity), combined, and concentrated for long-term storage at −80 °C. Protein concentrations of SOD samples were determined by the Bradford Method (Kruger 1994).

To obtain the pure and sole manganese occupied SOD_{cd}, M9 minimal medium was applied, which contains 2 mM $MgSO_4$, 0.1 mM $CaCl_2$, 0.00005 % thiamine and 0.4 % glucose as carbon source. The transformed strain was first amplified in 3 mL LB medium, then inoculated into 50 mL minimal medium, and last, transferred into 1 L minimal medium for over expression. 2 mM $MnCl_2$ was added into the M9 medium when the OD reaches to 0.5, and the expression was induced with 0.5 mM IPTG.

Characterization of $MnSOD_{cd}$

ICP-AES (Inductively Coupled Plasma-Atomic Emission Spectroscopy) was used to determine the metal content of $MnSOD_{cd}$ on Zeeman atomic absorption spectrometer (Z-5000, Hitachi, Japan). Metal standard solutions were purchased from Merck Labs.

Electronic absorption spectra of $MnSOD_{cd}$ were recorded on a HP8453 UV–visible spectrophotometer (*Agilent)*. X-band EPR spectra were recorded at 4 K on a Bruker EMX 300 equipped with an Oxford 900 cytostat and liquid helium as the coolant. The spectra were recorded under the following conditions: microwave frequency, 9.44 GHz; microwave power, 2.0 mW; modulation

frequency, 100 kHz; modulation amplitude, 4.00 G; and time constant, 163.84 ms. The SOD sample (0.5 mM) was prepared in 50 mM potassium phosphate (pH 7.8) containing 10 % glycerol. $MnSOD_{cd}$ was reduced by sub-stoichiometric H_2O_2 and quickly frozen in liquid N_2.

SOD activity assay

SOD activity was measured according to McCord and Fridovich's method (Crapo et al. 1978) using a 3 mL assay reaction cocktail containing 50 mM potassium phosphate, 0.1 mM ethylenediaminetetraacetic acid, 0.01 mM cyt *c*, 0.05 mM xanthine, and XO (sigma) used as the uninhibited control. The SOD activity inhibition of $MnSOD_{cd}$ by 2-ME was performed with 3 mL reaction solution containing the proper concentrations of $MnSOD_{cd}$, 2-ME, and XO (proper quantity). After quickly mixed at 25 °C, the absorbance at 550 nm was traced. The relative activity of $MnSOD_{cd}$ was calculated. Neither 2-ME nor DMSO (the solvent of 2-ME) affects the colorimetric reaction of cyt *c* in the absence of $MnSOD_{cd}$.

Crystallography of $MnSOD_{cd}$

The $MnSOD_{cd}$ enzyme (~15 mg/mL) was crystallized by hanging-drop vapor diffusion method at 16 °C under the following conditions: 0.2 M sodium citrate tribasic dehydrate and 20 % PEG 3350. The flash-cooled $MnSOD_{cd}$ crystal was mounted under a liquid N_2 stream, and diffraction data were collected from the single crystal on beamline BLXU17 at Shanghai Synchrotron Facility (SSRF) of China using a ADSC QUANTUM 315 detector with wavelength of 0.9792 Å at 100 K. The intensity data was processed using the program HKL2000 (Adams et al. 2010). For molecular replacement, the well-refined crystal structure of 1.6 Å structure of *B. subtilis* Superoxide Dismutase (PDB code 2RCV) (Liu et al. 2007) was used as the search model. Model building was done with the program Auto Build integrated into PHENIX (Terwilliger et al. 2008). For energy-restrained structure refinement, the maximum likelihood algorithms of CNS 36 were used (Paninski et al. 2004). The detailed statistics are showed in Table 1. Structural pictures were prepared using PyMOL (Pasi et al. 2012). Protein Data Bank accession number of $MnSOD_{cd}$ is 4JZG.

Isothermal titration calorimetry for the binding affinity between 2-ME and $MnSOD_{cd}$

To determine the stoichiometry of 2-ME binding with $MnSOD_{cd}$, the calorimetric titrations were performed with the MicroCal ITC_{200} instrument (Northampton, MA). The sample cell was held at 25 °C. The experimental buffer was 20 mM Tris–HCl (pH 7.4) containing 200 mM NaCl. The 0.1 mM $MnSOD_{cd}$ was fixed in the sample cell and 1 mM 2-ME was dissolved in 10 % DMSO in the injector. All solutions were degassed for 5–10 min prior to usage. After an initial addition of 0.4 μL of 2-ME solution, all subsequent additions were 2 μL with 120 s intervals between additions. Background data were collected by titrating 2-ME solutions into buffer blank and were subtracted from data obtained with the presence of $MnSOD_{cd}$. Titration data were fitted using Origin 7.0 software (OriginLab, Northampton, MA) integrated into the ITC software choosing the one single site binding mode.

Table 1 Summary of data collection and refinement statistics of $MnSOD_{cd}$

	$MnSOD_{cd}$
Wavelength	0.9795
Space group	$P6_522$
Unit-cell dimensions (Å, °)	$a = 80.592$, $b = 80.592$, $c = 249.509$ $\alpha = \beta = 90$, $\gamma = 120$
Resolution (Å)	2.32
No. of observations	363,844
No. of unique reflections	21,721 (1,055)[a]
Completeness (%)	99.9 (100.0)
$<I>/\sigma(I)$	37.5 (11.7)
Redundancy	16.7 (18.0)
R_{sym}^{b}	0.084 (0.370)
R_{cryst}^{c} (%)/R_{free}^{d} (%)	16.3/18.8
RMSD bonds (Å)/angles (°)	0.007/0.967
Ramachandran plot, residues in	
Most favored regions (%)	91.2
Additional allowed regions (%)	7.1
Generously allowed regions (%)	1.6
Disallowed regions (%)	0.0

[a] Numbers in parentheses represent values in the highest resolution shell (Å)

[b] $R_{sym} = \Sigma|I_j - <I>|/\Sigma I_j$, where I_j is the observed integrated intensity, $<I>$ is the average integrated intensity obtained from multiple measurements, and the summation is over all observed reflections

[c] $R_{cryst} = \Sigma||F_{obs}| - |F_{calc}||/\Sigma|F_{obs}|$, F_{obs} and F_{calc} are observed and calculated structure factor amplitudes, respectively

[d] R_{free} calculated with randomly selected reflections (5 %)

Results

Preparation and characterization of $MnSOD_{cd}$

The SOD_{cd} was expressed and purified as a MBP fusion protein, and the MBP tag was removed by TEV protease cleavage (Zhu et al. 2011; WE Blumberg 1967). The gel

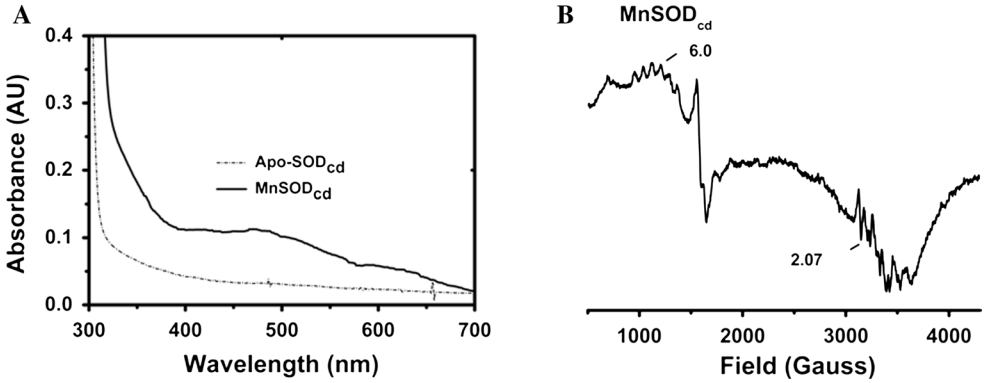

Fig. 1 The spectroscopic characterization of MnSOD$_{cd}$. **a** UV/Vis and **b** EPR for MnSOD$_{cd}$

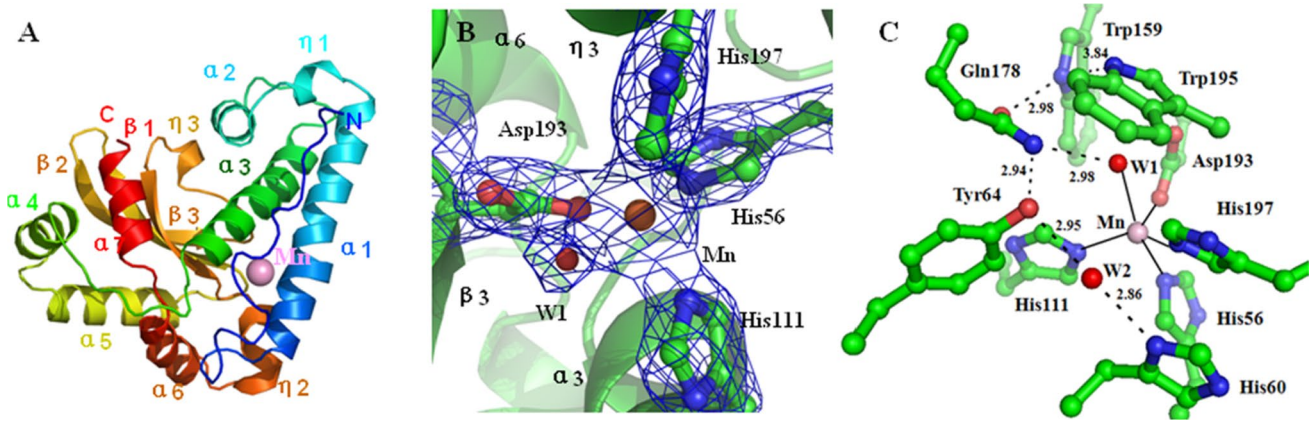

Fig. 2 Crystal structures of MnSOD$_{cd}$. **a** The overall structure of MnSOD$_{cd}$. **b** The 2Fo-Fc electron density map focused on the Mn-coordination sphere. **c** The hydrogen bond network around the metal center

filtration analysis indicated that the recombinant MnSOD$_{cd}$ exists as a dimer, similar to other bacterial SODs (Jackson and Cooper 1998) (Fig. S1). The authenticity of the purified SOD$_{cd}$ was further confirmed by the peptide finger spectrum (MS/MS spectrum) (Fig. S2). The pure/sole MnSOD$_{cd}$ was expressed in M9 minimal medium enriched with Mn^{2+} ions, and was purified in a strict metal-free buffer. Metal content analysis of MnSOD$_{cd}$ indicated an occupancy of 51 % for Mn^{2+}. It should be noted that the amounts of Mn were sub-stoichiometric in all reported cases, although the reason for this is not clear (Yamakura et al. 1995).

The spectroscopic characterization was further performed to confirm the manganese existence of the MnSOD$_{cd}$. The UV/Vis spectra (Fig. 1, panel A) showed that MnSOD$_{cd}$ has a maximum peak at 478 nm with a shoulder at 628 nm, which are similar to that of MnSOD (Cabelli et al. 1999) from *E. coli*. The EPR spectra of MnSOD$_{cd}$ (Fig. 1, panel B) showed six transitions at ~ 1,000 G ($g = 6.0$), which is due to the hyperfine structure that arose from the magnetic interaction of the electron spin ($S = 5/2$) on Mn(II) and the nuclear spin ($I = 5/2$) of ^{55}Mn (Maliekal et al. 2002).

Crystal structure of MnSOD$_{cd}$

2.32 Å Crystal structure of MnSOD$_{cd}$ was solved and details of the refinement statistics are presented in Table 1. The overall structure of MnSOD$_{cd}$ is composed of the α + β pattern and the metal coordination geometry of MnSOD$_{cd}$ is trigonal bipyramidal, with His111, His197 and Asp193 providing the equatorial ligands, and with His56 and the hydroxide or water forming the axial ligands (Fig. 2). The area around the active site is fairly hydrophobic with two encompassing tryptophan residues (159 and 195) being 5.43 and 5.24 Å from the metal, respectively. Trp159 forms a hydrogen bond with Gln178, which in turn forms a hydrogen bond with the phenolic oxygen of Tyr64. Tyr64 forms hydrogen bonds via a water molecule with His60, which is the gatekeeper residue responsible for controlling the substrate entering (Lah et al. 1995). Of particular interest comes from the dimer interface. As indicated in Fig. 3, there are three conserved communications involving three hydrogen bonds between Glu196 and His197, His60 and Tyr200, and another formed by Ser157 from the respective subunit. The structure indicates a close interaction of Glu196 and His197 between the two active sites,

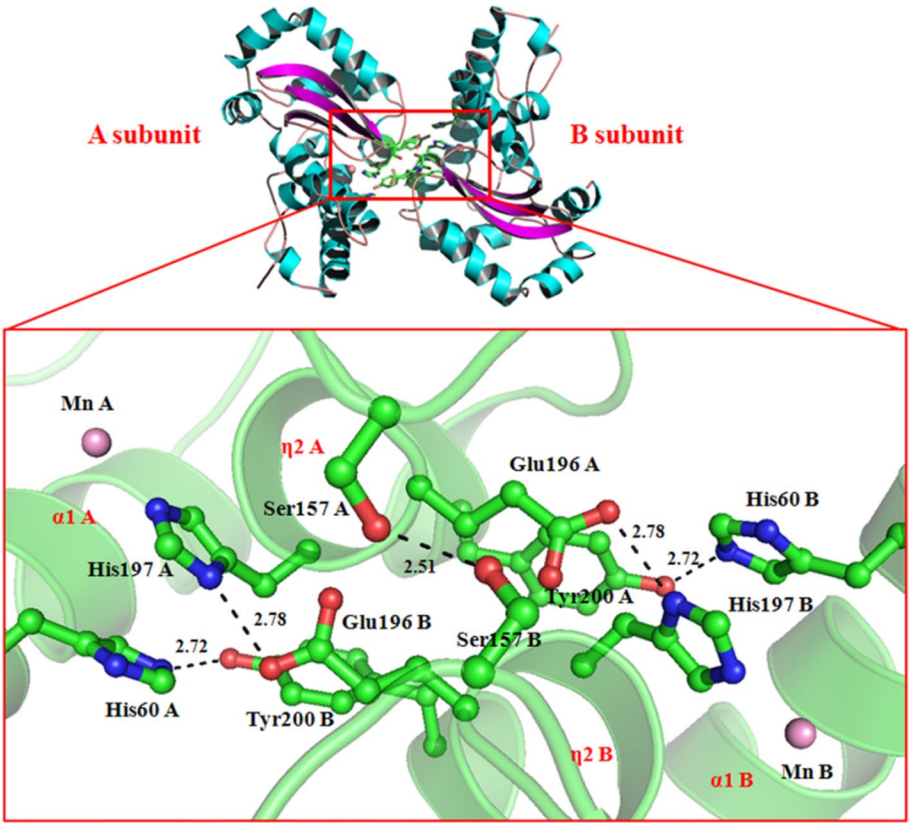

Fig. 3 The dimer of $MnSOD_{cd}$ focused on the interface. The *upper* and *below* pictures shows that the overall dimer packing and the local cross-links of $MnSOD_{cd}$. **a** and **b** Refer to each of $MnSOD_{cd}$ monomer

despite the fact that the enzyme is not known to exhibit cooperativity (Stallings et al. 1984).

$MnSOD_{cd}$, which is highly homologous to other MnSOD species (Jackson and Cooper 1998), exhibits similar peptide folding to other SOD species except that α1 connects to α3 directly in MnSOD from *H. sapiens*, while the α1 connects t α3 hrough α2 in $MnSOD_{cd}$ (Fig. S3). The average coordination bond distances of $MnSOD_{cd}$ are relatively longer than those in other MnSODs, especially for the distance of Mn-coordination solvent (2.35 Å) (Table 2). The second difference lies at the hydrogen bond between Gln178 and the coordination solvent, which is 2.93 Å in $MnSOD_{cd}$, compared with 3.03 Å in MnSOD from *P. gingivalis*, 2.77 Å in MnSOD from *H. sapiens*, respectively. This hydrogen bond plays an important role in tuning the redox potential of SOD and could partially be a discriminating factor for determining the type of Mn/Fe SOD.

Activity of $MnSOD_{cd}$ and its inhibition by 2-ME

The $MnSOD_{cd}$ activity, which was assayed using the XO/cyt *c* method (Crapo et al. 1978), exhibited 8,600 ± 50 U/mg. Notably, the activity of $MnSOD_{cd}$ from *C. difficile* is relatively higher than that of MnSOD (2,680 U/mg) from *H. sapiens*, MnSOD (3,300 U/mg) from *D. radiodurans* (Abreu et al. 2008), and MnSOD (6,000 U/mg) from *E. Coli* (Touati 1989).

The inhibitory investigation of $MnSOD_{cd}$ by 2-ME was performed based on the XO/cyt *c* method. As shown in Fig. 4, panel A, 1 μM of 2-ME exhibited a saturation inhibition effect on $MnSOD_{cd}$ (~1 μM), indicating preliminarily one molecular 2-ME binding to one monomer $MnSOD_{cd}$. Panel B showed that 2-ME exhibited a dose manner inhibition. Panel C showed the approximate value of IC_{50} for 2-ME is 75 μM. Panel D exhibited the blank control for this activity assay. The 2-ME alone and its solvent DMSO have no perturbation on the $MnSOD_{cd}$ activity assay.

The accurate binding stoichiometry between 2-ME and $MnSOD_{cd}$ was measured by ITC. As shown in Fig. 5 (upper panel A), upon titration of 2-ME, the system displayed substantial enthalpy changes ($\Delta H = -4.08 \pm 0.03$ kcal/mol, $\Delta S = 9.53 \pm 0.02$ cal/mol/deg). By fitting the profile of calorie compensation as a function of the molar ratio by the one site binding equation, the binding constant was calculated to be ~8.6 μM with the binding stoichiometry of ~1:1 (bottom panel A).

To probe the inhibitory mechanism of $MnSOD_{cd}$ by 2-ME, a computational molecular docking based on the crystal structure was performed. As indicated in Fig. S4, two favorable interaction patterns were suggested. One

Table 2 Bond distances and angles compared among the MnSOD from *C. difficile*, *H. sapiens*, *E.coli* and *P. gingivalis*, respectively

	MnSOD from *C. difficile* 4JZG	Cambialistic SOD from *P. gingivalis* 1QNN	Mn-specific SOD from *H. sapiens* 1LUV	Fe-specific SOD from *E.coli* 1ISB
Coordination bonds (Å)				
$M^1 - N^{\varepsilon 2}_{His56}$	2.20	2.14	2.20	2.15
$M - N^{\varepsilon 2}_{His111}$	2.08	2.13	2.28	2.06
$M - O^{2}_{Asp193}$	1.97	1.88	2.04	1.89
$M - N^{\varepsilon 2}_{His197}$	2.20	2.12	2.07	2.08
$M–O_{coordsolv}$	2.35	2.11	2.17	1.92
Coordination bond angles (°)				
$N^{\varepsilon 2}_{His197} - M - N^{\varepsilon 2}_{His56}$	93.13	93.22	88.56	90.66
$N^{\varepsilon 2}_{His56} - M - O^{2}_{Asp193}$	84.88	94.12	82.08	85.66
$O^{2}_{Asp193} - M - O_{coordsolv}$	79.62	86.57	90.55	91.60
$O_{coordsolv} - M - N^{\varepsilon 2}_{His111}$	95.70	89.85	93.77	89.17
$N^{\varepsilon 2}_{His111} - M - N^{\varepsilon 2}_{His197}$	132.42	134.39	133.92	128.40
Hydrogen bonds (Å)				
$O_{coordsolv} - O^{\delta 1}_{Asp193}$	2.85	3.05	2.91	3.03
$N^{\varepsilon 1}_{Gln178} - O_{coordsolv}$	2.93	3.03	2.77	3.48
$N^{\varepsilon 1}_{Gln178} - O^{\delta 1}_{Tyr64}$	2.86	3.10	2.98	3.10

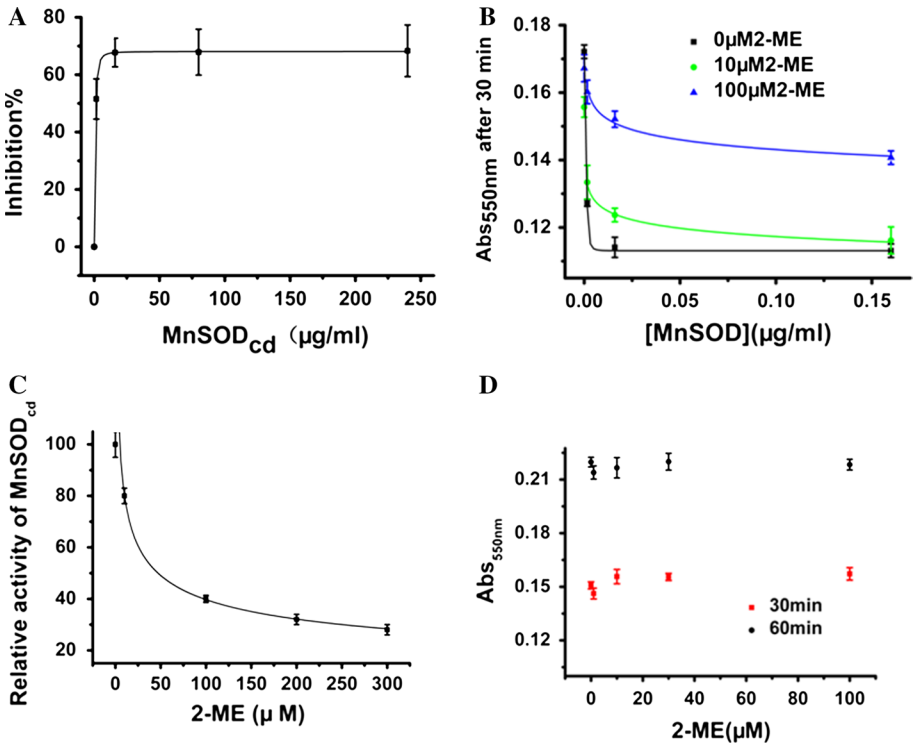

Fig. 4 MnSOD$_{cd}$ activity inhibited by 2-ME. **a** The inhibitory effect of 2-ME on MnSOD$_{cd}$ activity under different concentrations. **b** The inhibtion for MnSOD$_{cd}$ activity dependent on 2-ME concentration. **c** The approximate IC_{50} of 2-ME to inhibit MnSOD$_{cd}$ activity. Panel D, the blank control

binding model (panel A) showed that 2-ME adopted a chair conformation, which is held by a set of residues from α3 helix and the three typical β sheets as well as their linking loops, including Ser183, Lys184, Asp179, Thr174, Thr175 and Met173. Among which, Ser183, Lys184 and Thr174 are highly conserved in SODs (Jackson and Cooper 1998), indicating the important roles of these residues although they are not located in the first and second coordination spheres. The other binding model (panel B) showed that 2-ME, impressively inserted into the dimer interface of MnSOD$_{cd}$, endowed static electronic (salt bridge) interactions with Tyr200 and Glu196, which takes part in the

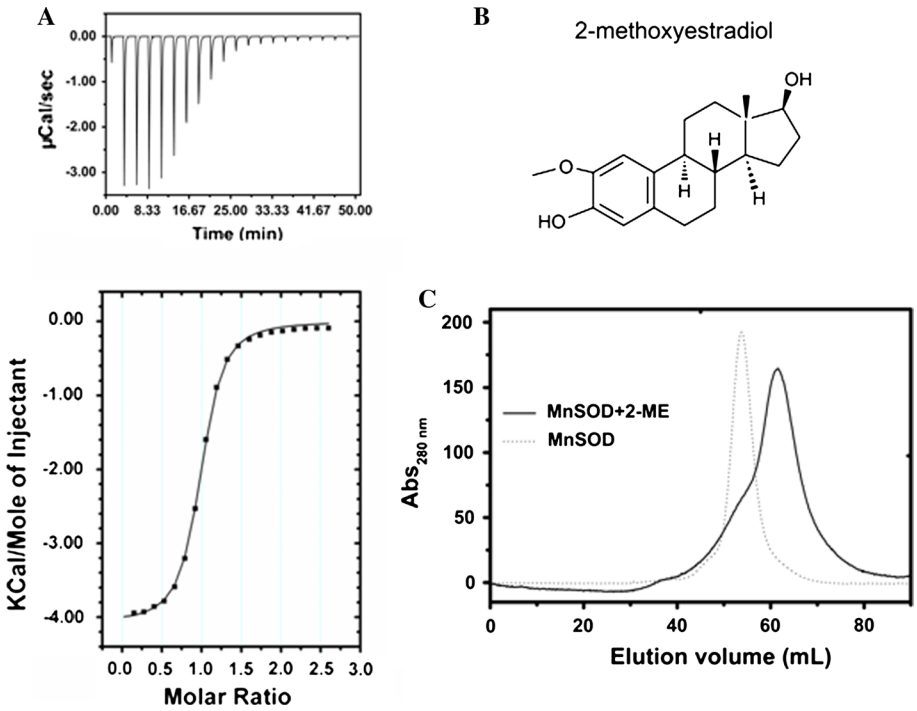

Fig. 5 The ITC and gel filtration analysis for 2-ME-$MnSOD_{cd}$ interaction. b The calorie compensation along with the addition of 2-ME and the curve fitting of the calorie changes as a function of molar ratios (2-ME: dimeric MnSOD). **b** The 2-D structure of 2-ME. **c** The gel filtration profiles of $MnSOD_{cd}$ in presence or absence of 2-ME by gel permeation chromatography using Superdex 75 column

crosslink of the two subunit's metal centers. In addition, the hydroxyl group of 2-ME formed hydrogen bonds with the metal coordinating residues His197 and Lys59, Ser157 and the carbonyl group of Gly156. Although these two models showed similar conformation scores (Table S1) and exhibited proper interactions with the SOD peptide, we incline to the second one based on the gel filtration analysis (Fig. 5, panel C), which indicated that 2-ME could disturb the dimer of $MnSOD_{cd}$ and disassemble it to its monomer species.

Discussion

Preparation and characteristic of $MnSOD_{cd}$

The metal center of SOD_{cd} can be occupied by Mn or Fe ions when expressed in TB media depending on the metal ions availability in the culture medium. The pure/sole $MnSOD_{cd}$ can be obtained using M9 minimal medium, enriched with Mn^{2+} ions. The SOD activity of pure $MnSOD_{cd}$ (8,600 U/mg) is much higher than that of an isolated impure Mn/$FeSOD_{cd}$ (3,020 U/mg) expressed in LB media. These results indicated that Mn ion is the native metal of the SOD_{cd}. In spite of high homolog of MnSOD and FeSOD, they could be exquisitely discriminated according to the primary sequence differences (Parker and Blake 1988). Although a few exceptions have been reported, these differences could be the primary candidates to account for the metal specificity of the Fe- and Mn-SOD family. An analysis of the primary residue sequence reveals that SOD_{cd} is a type of MnSOD. The sequence alignment of SOD_{cd} to other SODs was shown in Fig. S5. Lys54 of SOD_{cd} from the first α helix (KLHHDKHY) is the basic residue while other FeSODs and MnSODs normally have an acidic Glu residue or similar residues at this position (Jackson and Cooper 1998). The sequence of α3 helix (RNNAGGAYNHKFFF) is more representative of MnSODs. His111 is the second metal ligand and highly conservative across all the Fe/Mn SODs. Phe114 is conserved in MnSODs but changes to Tyr in FeSODs and that from *P. gingivalis* (Fig. S3) (Hiraoka et al. 2000). The only exception exists GWAWLVAT, where GW is typical of MnSODs but the Leu162 is conserved in FeSODs (Lancaster et al. 2004). The most discriminating residue is Gln178, which comes from the C-terminal of MnSODs but the N-terminal of FeSODs (Jackson and Cooper 1998). Gly191 is mostly found in MnSODs and cambialistic SODs, but it has changed to Thr in FeSODs (Fig. S3) (Yamakura et al. 2003). Briefly, the SOD_{cd} is representative of MnSODs, but meanwhile has mild characteristics of cambialistic SOD.

The inhibitor of $MnSOD_{cd}$

Although the overall structure of $MnSOD_{cd}$ is highly conserved among the Mn/Fe SOD family (Stallings et al. 1984), its subtly unique characteristics may allow the design of inhibitors to block the activity of $MnSOD_{cd}$ specifically without affecting other MnSODs. Human MnSOD is a homotetramer, while the prokaryotic MnSODs exhibits

a homodimer (Jackson and Cooper 1998). The human MnSOD polymorphic variant, Ile58Thr, reduces activity by destabilizing the tetrameric interface (Quint et al. 2006). Though comparing the crystal structures, we found the different linkage manners of α1 and α3 between $MnSOD_{cd}$ and *H. sapiens* MnSOD, which are important for tetrameric folding of *H. sapiens* MnSOD (Borgstahl et al. 1996). The dimer interface of $MnSOD_{cd}$ (Fig. 3) locates three communication pairs, i.e., His60A-Tyr200B, His60B-Tyr200A, Glu196A-His197B, Glu196B-His197A, and Ser157A-Ser157B, which were proposed to contribute to charge compensation for the buried metal ion and are important for SOD activity (Ludwig et al. 1991). It is reported that disturbing of the crosslink of Glu196-His197 at the dimer interface destabilized the dimer structure and changes the metal affinity (Whittaker and Whittaker 1998). Thus, the dimer interface should be an effective target region for developing potential inhibitors for $MnSOD_{cd}$.

2-ME can bind to $MnSOD_{cd}$ with a binding constant of ~ 8.6 μM and has a substantial inhibition effect with IC_{50} of ~ 75 μM. Based on the molecular docking simulation and the gel filtration results for the 2-ME-$MnSOD_{cd}$ complex, we suggest that 2-ME binds into the dimer interface and disturbs the communications of the two metal centers. The substantial enthalpy decreases along with 2-ME binding with $MnSOD_{cd}$ resulted from the hydroxyl and methoxyl group of 2-ME forming hydrogen bonds with the polar residues of $MnSOD_{cd}$ dimer interface. Meanwhile, other non-polar residues shield 2-ME in a relatively low dielectric environment, and thus, could result in some entropy penalties. The results provide valuable insights for mechanism-based inhibition strategies and further investigation by in vitro mutations and in vivo animal models.

Conclusion

The $MnSOD_{cd}$ from human pathogen *C. difficile*, for the first time, was prepared, and characterized by X-ray crystallography, UV/Vis and EPR spectroscopy, and activity assay, et al. The 2.32 Å crystal structure of $MnSOD_{cd}$ reveals a manganese coordination geometry of distorted trigonal bipyramidal with His111, His197, and Asp193 providing the equatorial ligands, and with His56 and a hydroxide or water forming the axial ligands. The activity of $MnSOD_{cd}$ can be effectively inhibited by 2-methoxyestradiol with IC_{50} of 75 μM. The affinity of 2-methoxyestradiol with $MnSOD_{cd}$ by ITC indicated a binding constant of 8.6 μM with enthalpy changes (ΔH, -4.08 ± 0.03 kcal/mol; ΔS, 9.53 ± 0.02 cal/mol/deg). The inhibitory model of MnSOD by 2-methoxyestradiol based on the molecular docking simulation, gel filtration analysis, and ITC studies was proposed. The 2-methoxyestradiol binds the interface of the $MnSOD_{cd}$ dimer, thus compromising the SOD activity. These results provide valuable insight for the rational design of $MnSOD_{cd}$ inhibitors for potential therapeutics for CDI.

Acknowledgments We sincerely thank Dr. Wei Tong from High Magnetic Field Laboratory of China Academy of Sciences, Prof. Jihu Su from University of Science and Technology, and Prof. Lindahl from Texas A&M University for EPR measurements and discussion. This work was financially supported partly by National Natural Science Foundation of China (No. 31270869, No. 21472027, No. 91013001), and the Ph.D. program of the Education Ministry of China (20100071110011).

Conflict of interest The authors declare that they have no competing financial interests.

References

Abreu IA, Hearn A, An H, Nick HS, Silverman DN, Cabelli DE (2008) The kinetic mechanism of manganese-containing superoxide dismutase from Deinococcus radiodurans: a specialized enzyme for the elimination of high superoxide concentrations. Biochemistry 47(8):2350–2356

Adams PD, Afonine PV, Bunkoczi G, Chen VB, Davis IW, Echols N, Headd JJ, Hung LW, Kapral GJ, Grosse-Kunstleve RW, McCoy AJ, Moriarty NW, Oeffner R, Read RJ, Richardson DC, Richardson JS, Terwilliger TC, Zwart PH (2010) PHENIX: a comprehensive Python-based system for macromolecular structure solution. Acta Crystallogr D Biol Crystallogr 66(Pt 2):213–221

Ambrose M, Gatti RA (2013) Pathogenesis of ataxia-telangiectasia: the next generation of ATM functions. Blood 121(20):4036–4045. doi:10.1182/blood-2012-09-456897

Blumberg WE (1967) The EPR of high spin $Fe3^+$ in rhombic fields. In: Ehrenberg A, Malmström BG, Vänngard T (eds) Magnetic resonance in biological systems. Pergamon, Oxford, pp 119–133

Borgstahl GE, Parge HE, Hickey MJ, Johnson MJ, Boissinot M, Hallewell RA, Lepock JR, Cabelli DE, Tainer JA (1996) Human mitochondrial manganese superoxide dismutase polymorphic variant Ile58Thr reduces activity by destabilizing the tetrameric interface. Biochemistry 35(14):4287–4297

Cabelli DE, Guan Y, Leveque V, Hearn AS, Tainer JA, Nick HS, Silverman DN (1999) Role of tryptophan 161 in catalysis by human manganese superoxide dismutase. Biochemistry 38(36):11686–11692

Chambergo FS, Valencia EY, Ferreira-Junior JR, Camilo CM, Campana PT (2012) Conformational stability of recombinant manganese superoxide dismutase from the filamentous fungus Trichoderma reesei. Int J Biol Macromol 50(1):19–24

Crapo JD, McCord JM, Fridovich I (1978) Preparation and assay of superoxide dismutases. Methods Enzymol 53:382–393

Fisher AE, Naughton DP (2005) Metal ion chelating peptides with superoxide dismutase activity. Biomed Pharmacother 59(4):158–162

Florczak U, Toulany M, Kehlbach R, Peter Rodemann H (2009) 2-Methoxyestradiol-induced radiosensitization is independent of SOD but depends on inhibition of Akt and DNA-PKcs activities. Radiother Oncol 92(3):334–338

Fridovich I (2011) Superoxide dismutases: anti- versus pro- oxidants? Anticancer Agents Med Chem 11(2):175–177

He D, Hagen SJ, Pothoulakis C, Chen M, Medina ND, Warny M, LaMont JT (2000) Clostridium difficile toxin A causes early damage to mitochondria in cultured cells. Gastroenterology 119(1):139–150

He D, Sougioultzis S, Hagen S, Liu J, Keates S, Keates AC, Pothoulakis C, Lamont JT (2002) Clostridium difficile toxin A triggers human colonocyte IL-8 release via mitochondrial oxygen radical generation. Gastroenterology 122(4):1048–1057

Herbst RW, Guce A, Bryngelson PA, Higgins KA, Ryan KC, Cabelli DE, Garman SC, Maroney MJ (2009) Role of conserved tyrosine residues in NiSOD catalysis: a case of convergent evolution. Biochemistry 48(15):3354–3369

Hiraoka BY, Yamakura F, Sugio S, Nakayama K (2000) A change of the metal-specific activity of a cambialistic superoxide dismutase from Porphyromonas gingivalis by a double mutation of Gln-70 to Gly and Ala-142 to Gln. Biochem J 2:345–350

Huang P, Feng L, Oldham EA, Keating MJ, Plunkett W (2000) Superoxide dismutase as a target for the selective killing of cancer cells. Nature 407(6802):390–395

Jackson SM, Cooper JB (1998) An analysis of structural similarity in the iron and manganese superoxide dismutases based on known structures and sequences. Biometals 11(2):159–173

Koo HL, Garey KW, Dupont HL (2010) Future novel therapeutic agents for Clostridium difficile infection. Expert Opin Investig Drugs 19(7):825–836

Kruger NJ (1994) The Bradford method for protein quantitation. Methods Mol Biol 32:9–15

Kuehne SA, Cartman ST, Heap JT, Kelly ML, Cockayne A, Minton NP (2010) The role of toxin A and toxin B in *Clostridium difficile* infection. Nature 467(7316):711–713

Lah MS, Dixon MM, Pattridge KA, Stallings WC, Fee JA, Ludwig ML (1995) Structure-function in Escherichia coli iron superoxide dismutase: comparisons with the manganese enzyme from Thermus thermophilus. Biochemistry 34(5):1646–1660

Lancaster VL, LoBrutto R, Selvaraj FM, Blankenship RE (2004) A cambialistic superoxide dismutase in the thermophilic photosynthetic bacterium Chloroflexus aurantiacus. J Bacteriol 186(11):3408–3414

Liu P, Ewis HE, Huang YJ, Lu CD, Tai PC, Weber IT (2007) Structure of Bacillus subtilis superoxide dismutase. Acta Crystallogr, Sect F: Struct Biol Cryst Commun 63(Pt 12):1003–1007

Ludwig ML, Metzger AL, Pattridge KA, Stallings WC (1991) Manganese superoxide dismutase from Thermus thermophilus. A structural model refined at 1.8 A resolution. J Mol Biol 219(2):335–358

Maliekal J, Karapetian A, Vance C, Yikilmaz E, Wu Q, Jackson T, Brunold TC, Spiro TG, Miller AF (2002) Comparison and contrasts between the active site PKs of Mn-superoxide dismutase and those of Fe-superoxide dismutase. J Am Chem Soc 124(50):15064–15075

Mallery SR, Pei P, Landwehr DJ, Clark CM, Bradburn JE, Ness GM, Robertson FM (2004) Implications for oxidative and nitrative stress in the pathogenesis of AIDS-related Kaposi's sarcoma. Carcinogenesis 25(4):597–603

Paninski L, Pillow JW, Simoncelli EP (2004) Maximum likelihood estimation of a stochastic integrate-and-fire neural encoding model. Neural Comput 16(12):2533–2561. doi:10.1162/0899766042321797

Parker MW, Blake CC (1988) Iron- and manganese-containing superoxide dismutases can be distinguished by analysis of their primary structures. FEBS Lett 229(2):377–382

Pasi M, Tiberti M, Arrigoni A, Papaleo E (2012) xPyder: a PyMOL plugin to analyze coupled residues and their networks in protein structures. J Chem Inf Model 5:5

Quint P, Ayala I, Busby SA, Chalmers MJ, Griffin PR, Rocca J, Nick HS, Silverman DN (2006) Structural mobility in human manganese superoxide dismutase. Biochemistry 45(27):8209–8215

Rupnik M, Wilcox MH, Gerding DN (2009) Clostridium difficile infection: new developments in epidemiology and pathogenesis. Nat Rev Microbiol 7(7):526–536

Scheinfeld N, Biggers K (2008) Tolevamer, an orally administered, toxin-binding polymer for Clostridium difficile-associated diarrhea. Curr Opin Investig Drugs 9(8):913–924

Sebaihia M, Wren BW, Mullany P, Fairweather NF, Minton N, Stabler R, Thomson NR, Roberts AP, Cerdeno-Tarraga AM, Wang H, Holden MT, Wright A, Churcher C, Quail MA, Baker S, Bason N, Brooks K, Chillingworth T, Cronin A, Davis P, Dowd L, Fraser A, Feltwell T, Hance Z, Holroyd S, Jagels K, Moule S, Mungall K, Price C, Rabbinowitsch E, Sharp S, Simmonds M, Stevens K, Unwin L, Whithead S, Dupuy B, Dougan G, Barrell B, Parkhill J (2006) The multidrug-resistant human pathogen Clostridium difficile has a highly mobile, mosaic genome. Nat Genet 38(7):779–786

Stallings WC, Pattridge KA, Strong RK, Ludwig ML (1984) Manganese and iron superoxide dismutases are structural homologs. J Biol Chem 259(17):10695–10699

Terwilliger TC, Grosse-Kunstleve RW, Afonine PV, Moriarty NW, Zwart PH, Hung LW, Read RJ, Adams PD (2008) Iterative model building, structure refinement and density modification with the PHENIX AutoBuild wizard. Acta Crystallogr D Biol Crystallogr 64(Pt 1):61–69

Touati D (1989) The molecular genetics of superoxide dismutase in E. coli. An approach to understanding the biological role and regulation of SODS in relation to other elements of the defence system against oxygen toxicity. Free Radic Res Commun 8(1):1–9

Whittaker MM, Whittaker JW (1998) A glutamate bridge is essential for dimer stability and metal selectivity in manganese superoxide dismutase. J Biol Chem 273(35):22188–22193

Williams OM, Spencer RC (2009) The management of *Clostridium difficile* infection. Br Med Bull 91:87–110

Yamakura F, Kobayashi K, Ue H, Konno M (1995) The pH-dependent changes of the enzymic activity and spectroscopic properties of iron-substituted manganese superoxide dismutase. Eur J Biochem 227(3):700–706. doi:10.1111/j.1432-1033.1995.0700p.x

Yamakura F, Sugio S, Hiraoka BY, Ohmori D, Yokota T (2003) Pronounced conversion of the metal-specific activity of superoxide dismutase from Porphyromonas gingivalis by the mutation of a single amino acid (Gly155Thr) located apart from the active site. Biochemistry 42(36):10790–10799

Zhang F, Zhu H (2006) Intracellular conformational alterations of mutant SOD1 and the implications for fALS-associated SOD1 mutant induced motor neuron cell death. Biochim Biophys Acta 3:404–414

Zhu X, Gu X, Zhang S, Liu Y, Huang ZX, Tan X (2011) Efficient expression and purification of methyltransferase in acetyl-coenzyme a synthesis pathway of the human pathogen *Clostridium difficile*. Protein Expr Purif 78(1):86–93